

# Supporting Information

## Two-Dimensional $\text{Bi}_2\text{Sr}_2\text{CaCu}_2\text{O}_{8+\delta}$ Nanosheets for Ultrafast Photonics and Optoelectronics

*Guanyu Liu,<sup>§,#</sup> Xiaozhi Bao,<sup>†,#</sup> Weikang Dong,<sup>‡</sup> Qi Wei,<sup>†</sup> Haoran Mu,<sup>¶</sup> Wenguo Zhu,<sup>◆</sup> Bingzhe Wang,<sup>†</sup> Jianding Li,<sup>†</sup> Babar Shabbir,<sup>¶</sup> Yuan Huang,<sup>△</sup> Guichuan Xing,<sup>†</sup> Jianhui Yu,<sup>◆</sup> Peng Gao,<sup>‡</sup> Huaiyu Shao,<sup>†\*</sup> Xiangping Li,<sup>§,\*</sup> and Qiaoliang Bao<sup>¶,\*</sup>*

G. Liu, Prof. X. Li

§ Guangdong Provincial Key Laboratory of Optical Fiber Sensing and Communications, Institute of Photonics Technology, Jinan University, Guangzhou, 510632, China

E-mail: xiangpingli@jnu.edu.cn

X. Bao, Q. Wei, B. Wang, J. Li, Prof. G. Xing, Prof. H. Shao

† Joint Key Laboratory of the Ministry of Education, Institute of Applied Physics and Materials Engineering, University of Macau, Macau SAR, 999078, China

E-mail: hshao@um.edu.mo

W. Dong, Prof. P. Gao

‡ International Center for Quantum Materials, and Electron Microscopy Laboratory, School of Physics, Peking University, Beijing, 100871, China

H. Mu, B. Shabbir, Prof. Q. Bao

¶ Department of Materials Science and Engineering, and ARC Centre of Excellence in Future Low-Energy Electronics Technologies, Monash University, Clayton, Victoria 3800, Australia

E-mail: [qiaoliang.bao@gmail.com](mailto:qiaoliang.bao@gmail.com)

W. Zhu, Prof. J. Yu

◆ Key Laboratory of Optoelectronic Information and Sensing Technologies of Guangdong Higher Educational Institutes, Jinan University, Guangzhou, 510632, China

Prof. Y. Huang

△ Institute of Physics, Chinese Academy of Sciences, Beijing, 100190, China

## 1. Pump-probe measurements

Infrared transient absorption measurements were performed using a Helios setup. The transient dynamics was acquired by Helios that works in a non-degenerate pump-probe configuration with femto-second to nano-second time resolution (50 fs – 7 ns). The pump pulses were generated from an optical parametric amplifier (OPerA Solo) that was pumped by a 1-kHz regenerative amplifier (Coherent Libra, 800 nm, 50 fs, 4 mJ). A mode locked Ti-sapphire oscillator (Coherent Vitesse, 80 MHz) was used to seed the amplifier. For pumping at 800 nm, the laser from the regenerative amplifier was directly used. The probe pulses were a white light continuum generated by passing the 800 nm femto-second pulses through a 1 cm sapphire plate for the operation in the infrared wavelength range (840–1600 nm). The pump incident light power intensity is  $1.15 \text{ GWcm}^{-2}$ . The transient absorption spectra pumped at 800 nm and probed at different wavelengths were shown in Figure S1(a). Figure S2(b) shows the carrier relaxation time *versus* probe wavelength. It can be seen that the carrier relaxation time (photohole lifetime) is inversely linear to probe photon energy (*i.e.*, almost linear to photon wavelength).

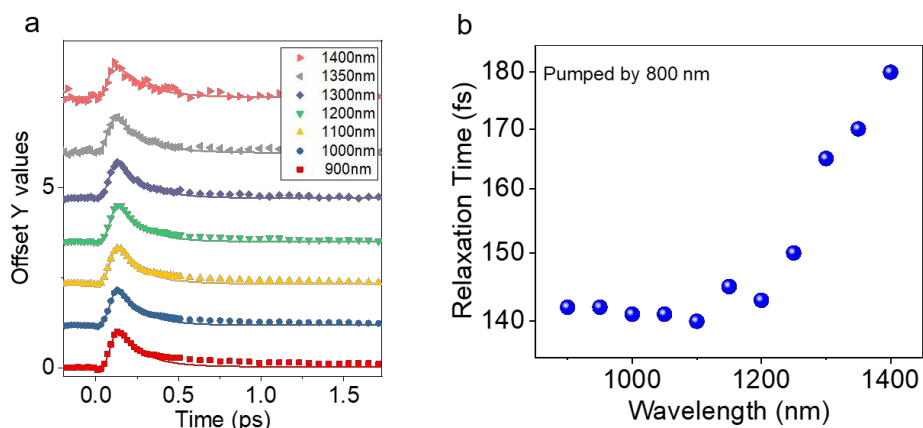


**Figure S1.** (a) Kinetic traces of Bi-2212 flake probed at different wavelengths. (b) Carrier relaxation time *versus* probe wavelength.

## 2. SA device fabrication

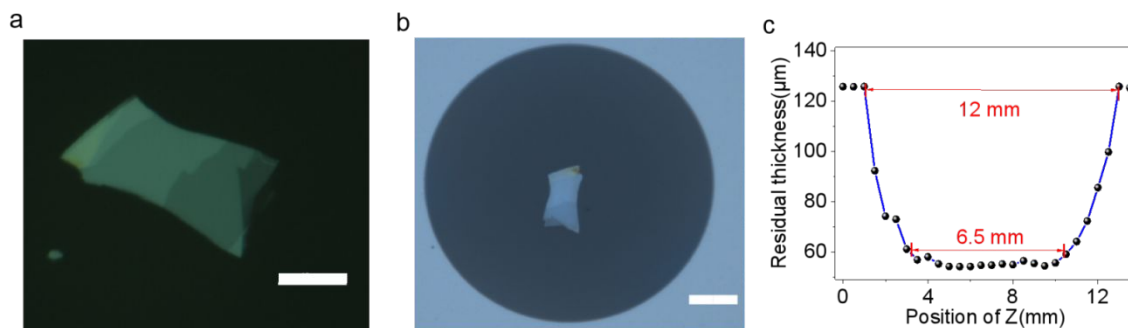


**Figure S2.** (a) 2D Bi-2212 flake on the surface of the viscoelastic PDMS substrate. Scale bar: 10  $\mu\text{m}$  (b) Optical image of 2D Bi-2212 flake covering the core area of the end facet of optical fiber ferrule. Scale bar: 20  $\mu\text{m}$ . (c) The residual thickness along the SPF as measured by optical microscope.

2D Bi-2212 flakes are mechanically exfoliated from bulk Bi-2212 single crystals (purchased from 2D SEMICONDUCTOR company) by using scotch tape. Then 2D Bi-2212 flakes were stamped onto polydimethylsiloxane (PDMS), as shown in Figure S2a, which is a key step for following material transfer. PDMS was selected as medium substrate due to its viscosity and transparency. The crystals were inspected through transparent PDMS substrate under an optical microscope before transferring so as to select the samples with suitable size and high quality. When the selected piece of Bi-2212 flake was aligned and in contact with the optical fiber ferrule (or the side polished fiber), the PDMS substrate was peeled off very gently and slowly. The selected 2D Bi-2212 flake will be separated from PDMS and adhered to the core area of fiber end-facet due to van der Waals force (see Figure S2b or inset of Figure S4a). It should be noted that the 2D Bi-2212 flake could keep intact after the dry transfer process.

A SPF was made from a single-mode fiber (SMF-28e) by wheel side-polishing technique. After polishing, the remaining SMF has a D-shaped cross-section. As shown in Fig. S2c, the residual thickness along the SPF was measured by microscope (Zeiss Axio Scope A1). A Bi-2212 nanosheet was transferred and attached onto the side polished fiber (SPF) as a SA device, as shown in inset of Figure 4a in main text and Figure S5a.

## 3. Nonlinear absorption measurements

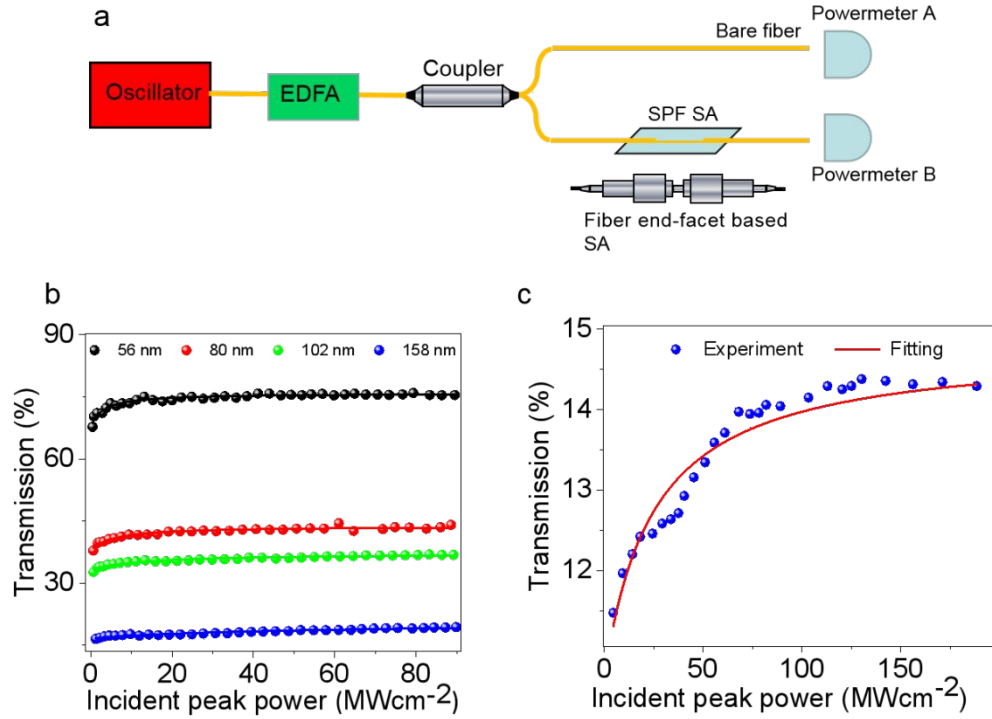


**Figure S3.** (a) Schematic of experimental setup for the nonlinear absorption measurements. (b) The nonlinear transmission of SA devices with different thicknesses of Bi-2212 flakes on the end-facet of optical fiber. The dots are the experimental data and the solid curves are analytical fits to the data using Equation (1). (c) Nonlinear transmission of Bi-2212 flake onto side-polished fiber. The globules are the experimental data and the solid curve is analytical fit to the data using Equation 1 in main text.

The nonlinear absorption measurement setup is schematically illustrated in Figure S3a. Stable and standard soliton mode locking fiber laser with output pulse width of 4.8 ps and repetition rate of 40 MHz was used as input pulse, which was then amplified by the erbium doped fiber amplifier (EDFA) and split into two patchcords with the same length by a coupler. To reduce the errors caused by the fluctuation of input power, the output powers (with or without passing through 2D Bi-2212 flake) were detected simultaneously through two sets of power meters with equal optoelectronic responses and parameter setups including sweeping time. Therefore, the difference of output power from power meter A and B gives the transmission loss due to the SA of the sample. The nonlinear transmission of Bi-2212 flakes with different thicknesses is shown in Figure S3b. We fit the data with equation (1) in the main text to obtain modulation depth and saturation intensity. The nonlinear transmission of the SPF SA is shown in Figure S3c. It also

exhibits characteristic saturable absorption property, *i.e.*, the transmittance increases with light intensity and gets flattened eventually. The modulation depth is measured as 2.9 %.

#### 4. Mode-locking using Bi-2212 on the fiber end-facet

Mode-locking state can be achieved using a SA device with a piece of 2D Bi-2212 nanosheet on the end-facet of optical fiber ferrule, as show in Figure S4. The mode-locked laser delivered pulses with an average power of 2.2 mW at a pump power of 580 mW. The output spectrum exhibits a triangular profile with the bandwidth of 1.02 nm, as shown in Figure S4a. The pulse train illustrated in Figure S4b shows that the repetition rate is 2.44 MHz. The intensity autocorrelation (AC) trace of the mode-locked pulses is shown in Figure S4c, which is well fitted by a  $\text{Sech}^2$  profile with a full-width at half-maximum (FWHM) of 3.24 ps. The broad band time scan range of the intensity autocorrelation is presented in inset of Figure S4c. A distinct basal envelope indicates that the laser is noise like mode locking. Due to the heating-effect, the mode-locking is unstable which can only maintain for a short time (about half an hour).

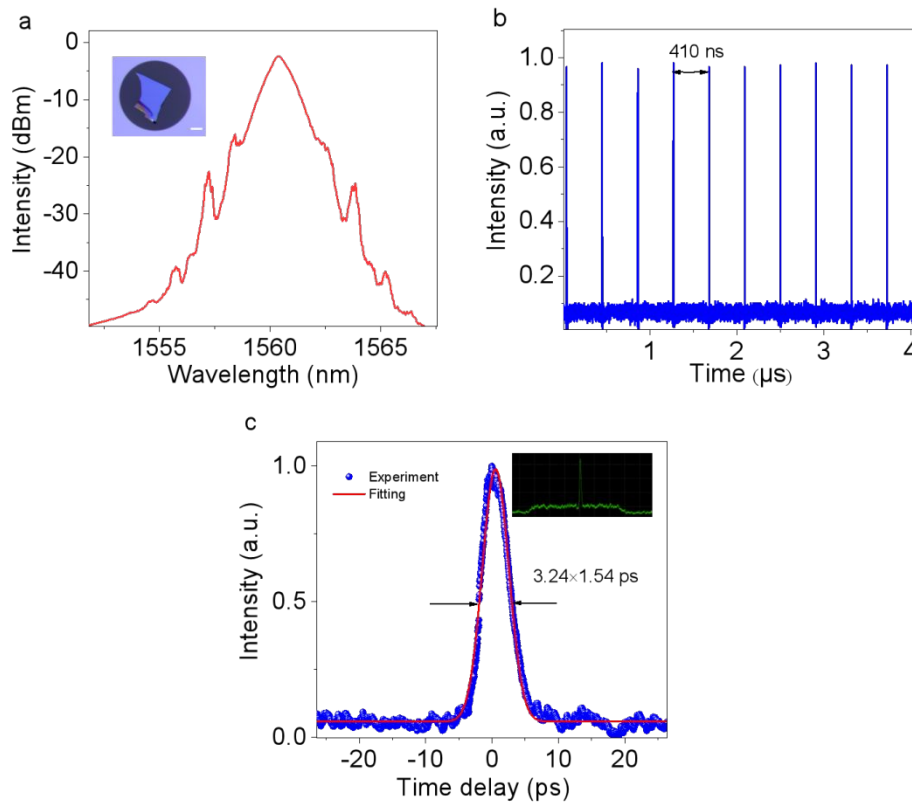


**Figure S4.** Characterizations of mode-locking state using Bi-2212 on the fiber end-facet. (a) Output optical spectrum. Inset: optical image of end-facet of optical fiber ferrule with a piece of 2D Bi-2212 flake covering the fiber core area. (b) Representative pulse train. (c) AC trace and Sech<sup>2</sup>fitting. The pulse width is 3.24ps. Inset: the wideband time scan range of the intensity autocorrelation.

**Table S1.** Comparison of mode locked fiber lasers at 1550 nm using various 2D material-SAs which include BSCCO, MXene, black phosphorus and TMDCs.

2D material SAs	Pulse width (ps)	Spectral (nm)	Central wavelength (nm)	Repetition rate (MHz)	Reference
$\alpha$ -Mo <sub>2</sub> C	1.81	1.66	1602.6	1.88	[1]
BP	2.18	1.25	1558.1	15.6	[2]
MoS <sub>2</sub>	1.28	2.6	1568.9	15.6	[3]
BSCCO	1.43	2.1	1559.5	3.17	This work

## 5. Q-switching state characterizations

In order to exclude the possibility of self-Q-switching of the fiber laser, the fiber laser operates without using the Bi-2212-based SA. It was found that only continuous wave emission was observed even when we increased the pump power to the maximum and/or adjusted the PC at all angles. Stable Q-switched laser pulses were produced from the fiber laser with a Bi-2212-based SPF SA (as shown in inset of Figure S5a) at a pumping power of from 395 mW to 840 mW. Figure S5 shows representative characteristics of the pulses output from Q-switched fiber laser. Typical Q-switching output spectrum is shown in Figure S5a, which indicates the central wavelength at 1558 nm. The measured radio-frequency (RF) spectrum is shown in Figure S5b which reveals a repetition rate of 57 kHz. Figure S5c shows the oscilloscope trace of the laser output and Figure S5c is the corresponding single pulse profile in time domain with a narrower sweep span. The pulse has a FWHM of 2.87  $\mu$ s. Power dependent repetition rate and average power of output pulses were also recorded, as shown in Figure S5e. With the increase of the pump power from 395 mW to 840 mW, the repetition rate of pulses increases from 49.1 kHz to 66 kHz and the average power increases from 0.53 mW to 1.16 mW,.

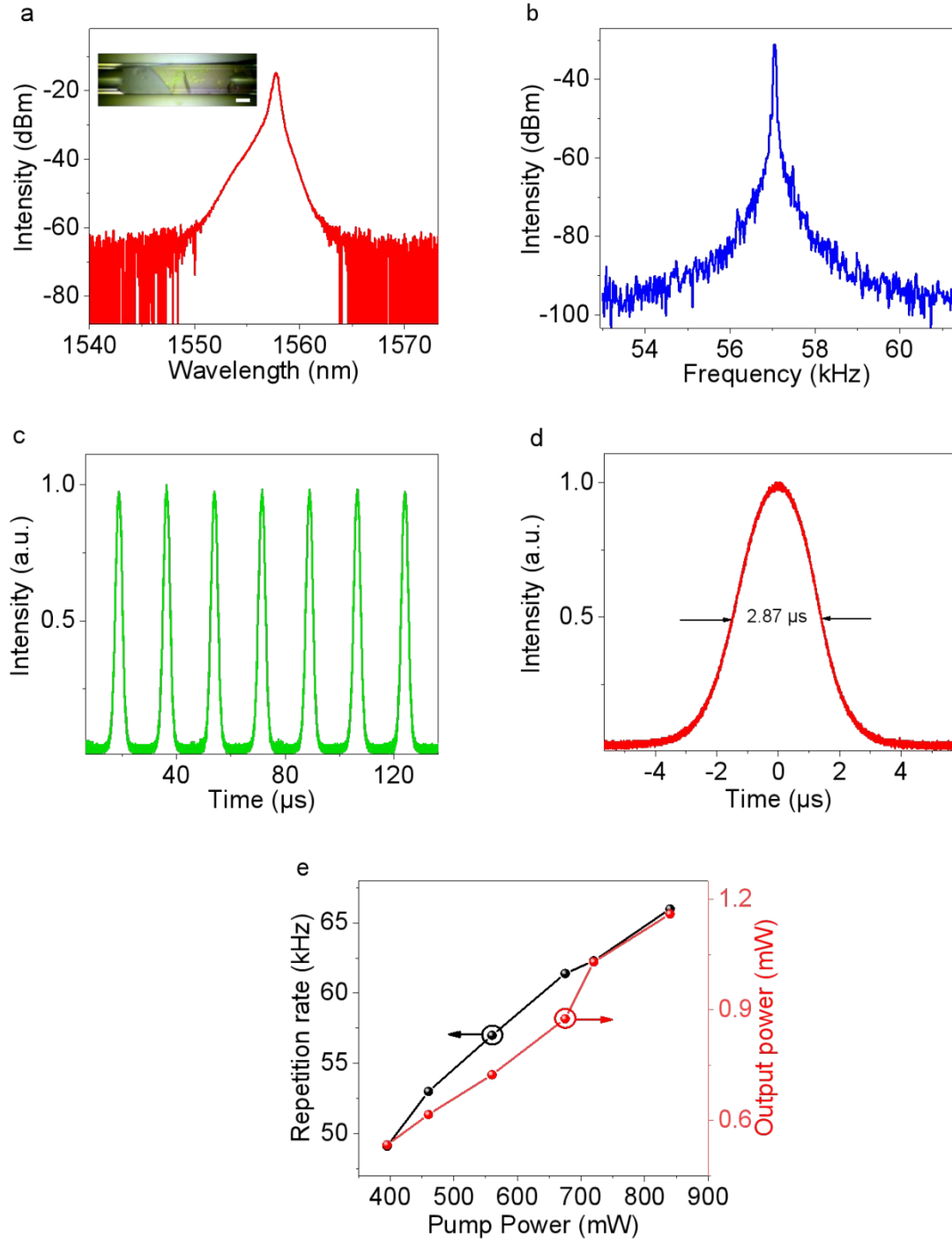


**Figure S5.** Q-switching output pulse characteristics. (a) Typical output spectrum centered at 1558 nm. Inset: photograph of a SPFL SA. Scale bar: 50  $\mu\text{m}$ . (b) Radio frequency spectrum. (c) Output pulse train. (d) Profile of single Q-switching pulse. (e) Pulse repetition rate and output power as a function of incident pump power.

## 6. FCPD fabrication and characterization

The fabrication of the FCPD is schematically illustrated in Figure S6. Initially, a ~50 nm thick gold film was deposited on the SiO<sub>2</sub>/Si substrate and transferred on the polydimethylsiloxane (PDMS). We can always find some natural gaps of the gold film on the PDMS which were formed during the peeling off process due to the incomplete detachment of the gold film from the SiO<sub>2</sub>/Si substrate, as shown in Figure S7a-b. Then, the parallel gap structures were aligned and transferred onto the cross-section of fiber pigtail, as shown in Figure S7c-d. Two separate parts of the parallel gap structure will function as two electrodes for photodetector. A tapered tungsten tip was used to scratch and clean the channel region in the gap under an optical microscope. The tungsten tip was fixed on a high precision translation stage. After that, 2D Bi-2212 nanosheets were mechanically exfoliated from bulk Bi-2212 single crystals and stamped onto PDMS, as shown in Figure S7e. We transferred the 2D Bi-2212 nanosheet across two gold electrodes and aligned it to the whole fiber core area (see Figure S7f). The whole fabrication process was performed under an optical microscopy with the help of a high precision translation stage.

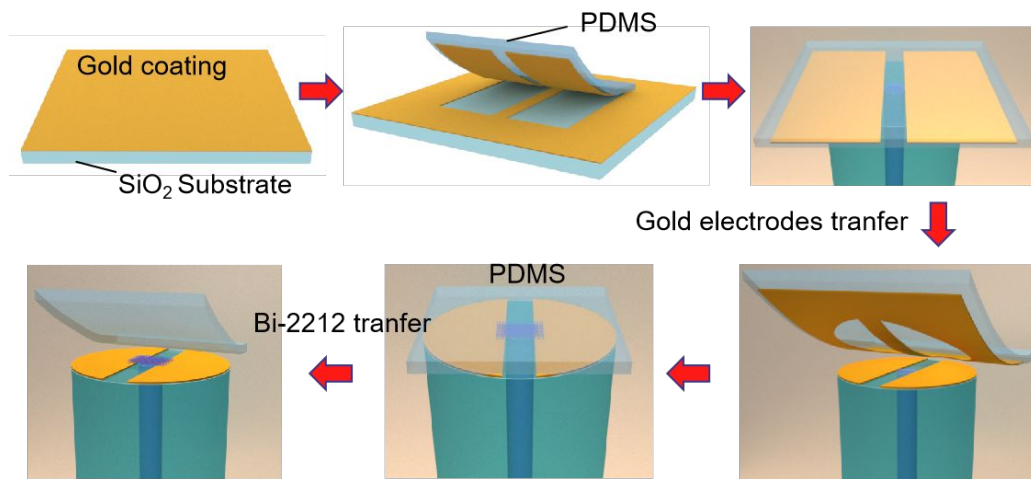


**Figure S6.** Schematics of the fabrication process of the FCPD. Gold film was deposited on the SiO<sub>2</sub>/Si substrate and transferred on the PDMS by leaving gap structures. Then, the gap structure was aligned and transferred from the SiO<sub>2</sub> substrate to the core area of fiber pigtail end-facet. After that, a 2D Bi-2212 nanosheet was transferred across two electrodes and make sure it covered the whole fiber core area.

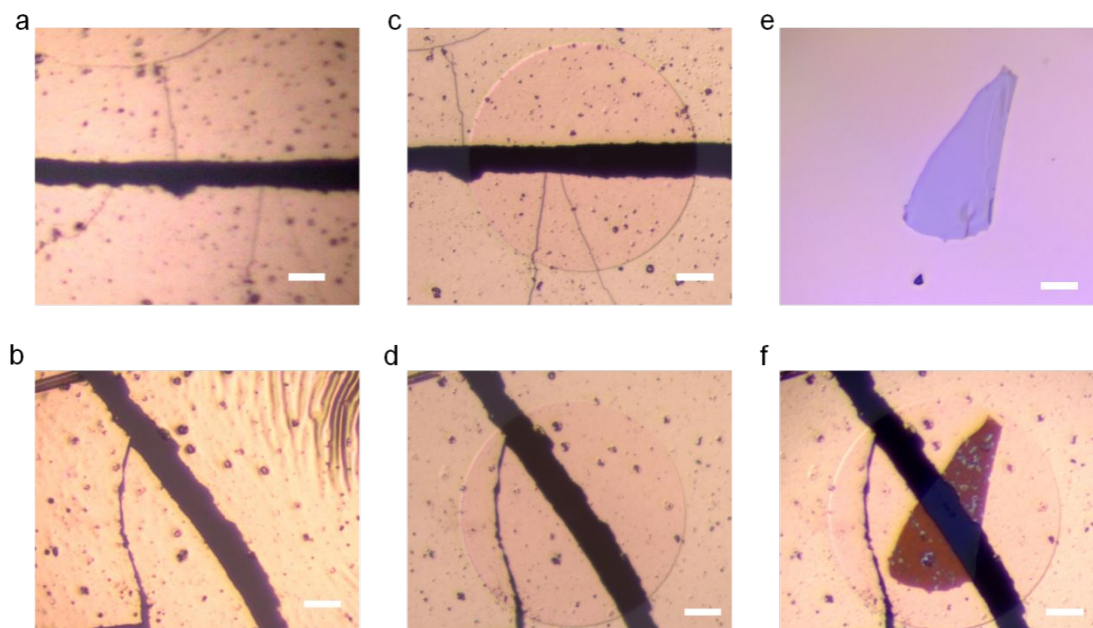


**Figure S7.** (a) and (b) Optical images of the parallel gap structures of gold film on PDMS substrate. Scale bar: 20  $\mu\text{m}$ . (c) and (d) Optical images of the parallel gap structures transferred onto the cross-section of fiber pigtail. Scale bar: 20  $\mu\text{m}$ . (e) Optical images of a 2D Bi-2212 nanosheet on PDMS substrate. Scale bar: 20  $\mu\text{m}$ . (f) Optical image of the as-fabricated FCPD. Scale bar: 20  $\mu\text{m}$ .

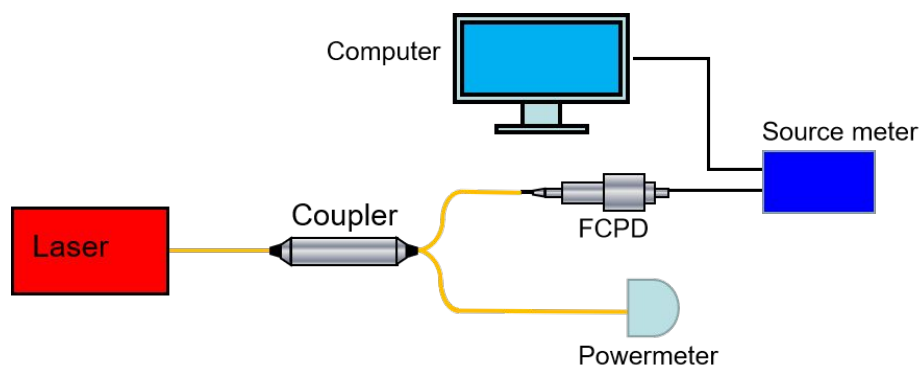


**Figure S8.** Schematic illustration of the photoelectrical characterization of FCPD.

The source light can be coupled into the optical fiber and directly projected to the FCPD at the output port without any lens system, because our photodetector was fabricated on the end-facet of the optical fiber, which is different from a conventional field-effect transistor (EET) on silicon. A double-arm configuration is used to calibrate the input light power passing through the FCPD, as illustrated in Figure S8. The Keithley source meter (Keithley2450) controlled by Labview programs was employed to exert voltage bias and analyze the current simultaneously.

## REFERENCES

- (1) Tuo, M.; Xu, C.; Mu, H.; Bao, X.; Wang, Y.; Xiao, S.; Ma, W.; Li, L.; Tang, D.; Zhang, H.; Premaratne, M.; Sun, B.; Cheng, H.-M.; Li, S.; Ren, W.; Bao, Q. Ultrathin 2D Transition Metal Carbides for Ultrafast Pulsed Fiber Lasers. *ACS Photonics* **2018**, *5*, 1808-1816.
- (2) Mu, H.; Lin, S.; Wang, Z.; Xiao, S.; Li, P.; Chen, Y.; Zhang, H.; Bao, H.; Lau, S. P.; Pan, C.; Fan, D.; Bao, Q. Black Phosphorus–Polymer Composites for Pulsed Lasers. *Adv. Opt. Mater.* **2015**, *3*, 1447-1453.
- (3) Xia, H.; Li, H.; Lan, C.; Li, C.; Zhang, X.; Zhang, S.; Liu, Y. Ultrafast Erbium-Doped Fiber Laser Mode-Locked by a CVD-Grown Molybdenum Disulfide (MoS<sub>2</sub>) Saturable Absorber. *Opt. Express* **2014**, *22*, 17341-17348.